

On the carriers of the 21 μm emission feature in post-asymptotic giant branch stars

Ke Zhang,^{1*} B. W. Jiang^{1,2*} and Aigen Li^{2*}

¹*Department of Astronomy, Beijing Normal University, Beijing 100875, China*

²*Department of Physics and Astronomy, University of Missouri, Columbia, MO 65211, USA*

Accepted 2009 March 21. Received 2009 March 21; in original form 2009 January 6

ABSTRACT

The mysterious 21 μm emission feature seen in sixteen C-rich proto-planetary nebulae (PPNe) remains unidentified since its discovery in 1989. Over a dozen of materials are suggested as the carrier candidates. In this work, we quantitatively investigate eight inorganic and one organic carrier candidates in terms of elemental abundance constraints, while previous studies mostly focus on their spectral profiles (which could be largely affected by grain size, shape and clustering effects). It is found that: (1) five candidates (TiC nanoclusters, fullerenes coordinated with Ti atoms, SiS₂, doped-SiC and SiO₂-coated SiC dust) violate the abundance constraints (i.e. they require too much Ti, S or Si to account for the emission power of the 21 μm band), (2) three candidates (carbon and silicon mixtures, Fe₂O₃ and Fe₃O₄), while satisfying the abundance constraints, exhibit secondary features which are not detected in the 21 μm sources and (3) nano FeO, neither exceeding the abundance budget nor producing undetected secondary features, seems to be a viable candidate, supporting the suggestions of Posch, Mutschke & Andersen.

Key words: stars: AGB and post-AGB – circumstellar matter – stars: individual: HD 56126 – infrared: stars.

1 INTRODUCTION

Since its first detection in 1989 (Kwok, Volk & Hrivnak 1989), the so-called ‘21 μm feature’ has been identified in 16 proto-planetary nebulae (PPNe; Kwok, Volk & Hrivnak 1999; Hrivnak, Volk & Kwok 2009) [and arguably also in two planetary nebulae (PNe) associated with Wolf–Rayet central stars (Hony, Waters & Tielens 2001) and in two highly evolved carbon stars (Volk, Xiong & Kwok 2000)]. This feature has little shape variation among different sources with a peak wavelength at $\sim 20.1 \mu\text{m}$ and a full width at half-maximum (FWHM) of $\sim 2.2\text{--}2.3 \mu\text{m}$. Most of these sources exhibit quite uniform characteristics: they are metal-poor, carbon-rich F and G supergiants with strong infrared (IR) excess and over abundant s-process elements (Zhang, Jiang & Li 2006).

After its discovery, over a dozen of carrier candidates have been proposed (see Fig. 1), with the number of proposed candidate materials comparable to the total number of the 21 μm feature sources (see Andersen et al. 2005; Zhang et al. 2006). These include both inorganic materials: (a) TiC nanoclusters (Von Helden et al. 2000), (b) SiS₂ grains (Goebel 1993), (c) Doped-SiC dust (Speck &

Hofmeister 2004), (d) carbon and silicon mixtures (Kimura et al. 2005), (e) SiC core-SiO₂ mantle grains (Posch et al. 2004), (f) FeO (Posch et al. 2004), (g) Fe₂O₃ and (h) Fe₃O₄ (Cox 1990); and organic materials: (i) large-cage carbon particles (fullerenes) coordinated with Ti atoms (Kimura, Nuth & Ferguson 2005), (j) urea or thiourea (Sourisseau, Coddens & Papoular 1992), (k) polycyclic aromatic hydrocarbon (PAH) and (l) hydrogenated amorphous carbon (HAC) (Buss et al. 1993; Justtanont et al. 1996).

However, the carrier of this feature remains unidentified (see Posch et al. 2004 for an excellent overview). It is considered as one of the most interesting unresolved mysteries in astrochemistry (Kwok, Volk & Hrivnak 2002). Previous studies mostly rely on a comparison of the spectral profile of a candidate material with the observed 21 μm emission feature. In this respect, astronomers often consider spherical dust using Mie theory. However, the spectral profile is expected to vary with grain shape, size and the presence of voids (e.g. see Huffman 1989; Li, Shi & Li 2008; Voshchinnikov & Henning 2008). Although models based on spherical dust may not fit the observed 21 μm emission feature, one cannot rule out the possibility that a reasonably good fit may be obtained by fine-tuning dust shape and size distributions. Indeed, some studies have demonstrated that the spectral fit is improved with a continuous distribution of ellipsoids (CDE; see e.g. Posch et al. 2004) for the dust shape. We should note that even the failure of

*E-mail: zhangke@mail.bnu.edu.cn (KZ); bjiang@bnu.edu.cn (BWJ); lia@missouri.edu (AL)

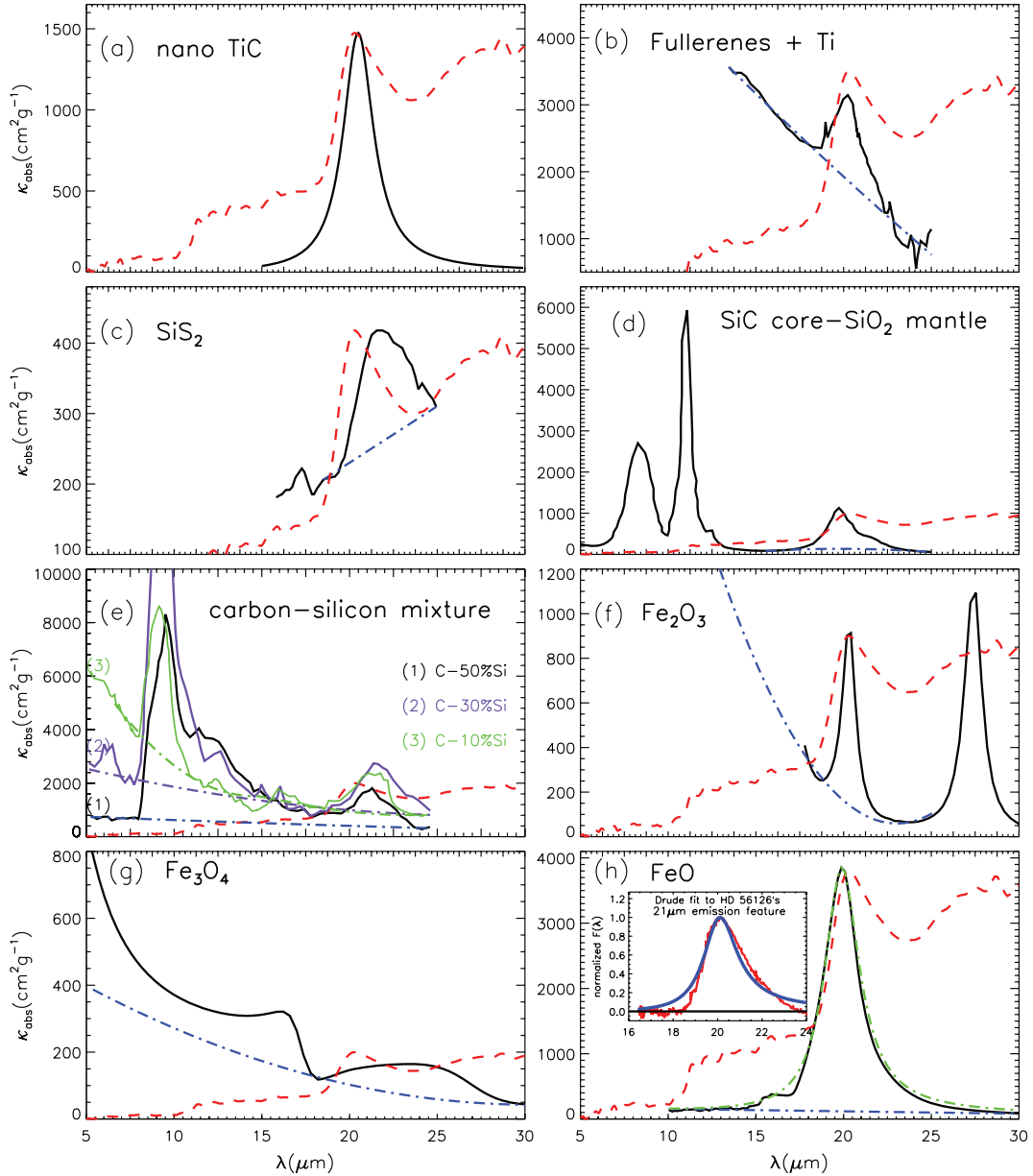


Figure 1. Experimental or calculated mass absorption coefficient spectra $\kappa_{\text{abs}}(\lambda)$ (black solid line) in the 21 μm wavelength range of eight carrier candidates for the 21 μm feature seen in PPNe: (a) TiC nanoclusters, (b) large-cage carbon particles (fullerenes) coordinated with Ti atoms, (c) SiS_2 dust, (d) SiC core-SiO₂ mantle dust, (e) carbon and silicon mixtures, (f) Fe_2O_3 , (g) Fe_3O_4 and (h) FeO. Also shown is the astronomical emission spectrum of HD 56126 (scaled to match the κ_{abs} peak at 21 μm ; red dashed line), a proto-typical 21 μm feature source. The blue dot-dashed line plots the continuum underneath the experimental (or calculated) 21 μm mass absorption spectrum. Also shown in (h) is the Drude fit (with $\lambda_p = 20.1$ μm and $\gamma = 2.4$ μm ; green dot-dashed line) to the mass absorption profile $\kappa_{\text{abs}}(\lambda)$ of FeO calculated from Mie theory (solid black line). The inserted panel in (h) fits the normalized, continuum-subtracted 21 μm emission feature of HD 56126 (solid red line) by $\kappa_{\text{abs}}(\lambda) B_\lambda(T)$, the product of a Drude mass absorption profile (with $\lambda_p = 20.1$ μm and $\gamma = 1.85$ μm) and a blackbody of $T = 90$ K (solid blue line; see Footnote 1).

CDE models cannot readily rule out the considered candidate material since the spectral profile could be further affected by many other factors (e.g. clustering of individual grains, see Rouleau & Martin 1991).

In this work, we attempt to constrain the nature of the 21 μm feature carrier by performing a systematic study of the validity of the above-listed candidate carriers. In view of the fact that a spectral profile ‘mismatch’ could probably be improved by considering dust shape and size distributions, clustering of individual grains, and the

presence of voids, unlike previous studies, we do not completely rely on whether the interested candidate material produces a band profile closely matching the observed one. Instead, we take an alternative approach which at least complements previous approaches (which are mainly based on spectral profile matching): we focus on the elemental abundance required to account for the total power emitted in the 21 μm feature. This approach is less affected by the (unknown) dust clustering and shape distribution and is therefore more robust.

This paper is organized as follows: we first present in Section 2 the general constraints on the validity of a proposed carrier. We then apply these constraints to the above-listed candidate materials (Section 4). For this purpose, we choose the prototypical 21 μm feature source HD 56126 as a comparison basis. The main results are summarized in Section 5.

2 GENERAL CONSTRAINTS: BAND STRENGTH AND ABUNDANCE BUDGET

For a candidate carrier to be a viable explanation of the 21 μm feature, in addition to the close match with the 21 μm feature observed in PPNe, it must satisfy the abundance constraint, i.e. the candidate material must be abundant enough to account for the total power emitted in the 21 μm feature. Further, it should of course not produce any secondary features which are not observed in the 21 μm sources.

The 21 μm feature is one of the strongest IR dust features in C-rich evolved objects. The strongest 21 μm source (HD 56126) emits ~ 8 per cent of its total IR power in this feature, while the 21 μm feature in other sources amounts to ~ 1 –7 per cent of their total IR power (Hrivnak, Volk & Kwok 2000). That the 21 μm feature emits such a large energy would put stringent constraint on the abundance of the carrier, particularly, on the abundance of the relatively rare element in the suggested carrier material (e.g. Ti in TiC).

Let E_{tot} be the total power emitted in the 21 μm band, which is an observational parameter. It is related to the total mass of the carrier dust M_d through

$$E_{\text{tot}} = M_d \int_{21 \mu\text{m band}} \kappa_{\text{abs}}(\lambda) \times 4\pi B_\lambda(T_d) d\lambda, \quad (1)$$

where the integration is over the 21 μm band (but with the continuum underneath the 21 μm feature subtracted), κ_{abs} is the mass absorption coefficient (also known as ‘opacity’) of the dust, $B_\lambda(T_d)$ is the Planck function of a blackbody with temperature T_d at wavelength λ and T_d is the dust temperature.

If the carrier material contains element X, the abundance of element X (relative to H) in the dust can be written as

$$[X/H] = \frac{n_X M_d / \mu_d m_H}{M_H / m_H}, \quad (2)$$

where M_H is the total hydrogen mass of the circumstellar envelope of the object, m_H is the mass of a hydrogen atom, μ_d is the molecular weight of the dust grain, and n_X is the number of atoms per molecule for element X. With a good knowledge of the dust temperature and the mass absorption coefficient in the 21 μm wavelength range of the carrier, one can therefore estimate the abundance of a typical element locked up in dust required to emit the observed power E_{tot} in the 21 μm band

$$[X/H] = \frac{n_X E_{\text{tot}}}{\mu_d M_H \int_{21 \mu\text{m band}} \kappa_{\text{abs}}(\lambda) \times 4\pi B_\lambda(T_d) d\lambda}. \quad (3)$$

It can be seen that for a given E_{tot} , the required abundance $[X/H]$ is inversely proportional to the integral of absorption coefficient κ_{abs} and the dust radiation intensity $B_\lambda(T_d)$ over the 21 μm band range.

We approximate the mass absorption coefficient profile with a Drude function

$$\kappa_{\text{abs}}(\lambda) = \frac{\kappa_{\text{abs}}^{\text{int}} 2\gamma/\pi}{(\lambda - \lambda_p^2/\lambda)^2 + \gamma^2}, \quad (4)$$

where $\lambda_p \approx 20.1 \mu\text{m}$ and $\gamma \approx 2.2 \mu\text{m}$ are, respectively, the peak wavelength and FWHM of the profile,¹ and $\kappa_{\text{abs}}^{\text{int}} \equiv \int_{21 \mu\text{m band}} \kappa_{\text{abs}}(\lambda) d\lambda$ is the mass absorption coefficient integrated over the 21 μm band. The adoption of a Drude function and the values of λ_p and γ which match the observed feature profile mostly is the best condition for the absorption coefficient. The abundance under such condition is the minimum. By substituting equation (4) into equation (3), the lower limit of $[X/H]$ becomes

$$[X/H]_{\text{min}} = \frac{n_X E_{\text{tot}}}{8\mu_d M_H \gamma \kappa_{\text{abs}}^{\text{int}} \int_{21 \mu\text{m band}} \{B_\lambda(T_d) / [(\lambda - \lambda_p^2/\lambda)^2 + \gamma^2]\} d\lambda}. \quad (5)$$

Note that the integration is continuum-subtracted. Since the Planck function $B_\lambda(T)$ is a monotonically increasing function of T_d , the minimum abundance of element X, $[X/H]_{\text{min}}$, becomes a decreasing function of T_d and $\kappa_{\text{abs}}^{\text{int}}$. For a fixed E_{tot} , given a reasonable dust temperature range [usually ~ 100 –200 K for the circumstellar envelope of post-asymptotic giant branch (post-AGB) stars] and $\kappa_{\text{abs}}^{\text{int}}$ from laboratory data, we can estimate the range of $[X/H]_{\text{min}}$. For a viable candidate, the required minimum abundance $[X/H]_{\text{min}}$ must not exceed what is available.

If $\kappa_{\text{abs}}(\lambda)$ is measured in the laboratory, $\kappa_{\text{abs}}^{\text{int}}$ can be obtained from the direct integration of the measured profile of $\kappa_{\text{abs}}(\lambda)$. In a few cases, $\kappa_{\text{abs}}(\lambda)$ is not directly measured, we obtain $\kappa_{\text{abs}}^{\text{int}}$ from the absorption cross-section C_{abs} or the absorption efficiency Q_{abs} calculated through Mie theory

$$\begin{aligned} \kappa_{\text{abs}}^{\text{int}} &= \int_{21 \mu\text{m band}} \kappa_{\text{abs}}(\lambda) d\lambda \\ &= \int_{21 \mu\text{m band}} \frac{C_{\text{abs}}(a, \lambda)}{M} d\lambda \\ &= \frac{3}{4\rho_d} \int_{21 \mu\text{m band}} \frac{Q_{\text{abs}}(a, \lambda)}{a} d\lambda, \end{aligned} \quad (6)$$

where M and a are, respectively, the mass and radius of the dust grain (we assume that the dust is spherical), and ρ_d is the mass density of the dust.

3 THE TESTER: HD 56126

A successful candidate carrier should be able to explain the observed 21 μm feature in all sources. A failure in a single source would be sufficient to rule out the candidate. To examine whether the carriers can account for the observed feature strength, we choose HD 56126, a prototypical 21 μm feature source, as the tester.

¹ The Drude profile, closely resembling a Lorentz profile and having more extended wings than a Gaussian profile, is expected for classical damped harmonic oscillators (Li 2008). With $\lambda_p = 20.1 \mu\text{m}$ and $\gamma = 2.2 \mu\text{m}$, the Drude profile fits well the observed 21 μm emission feature except the blue-wing (which is a bit more extended than that observed), while the Gaussian profile is a bit too narrow in the red-wing. To be more physical, we should fit the observed 21 μm emission feature with $\sum_j \kappa_{\text{abs}}(\lambda) B_\lambda(T_j)$, a sum of products of a Drude mass absorption profile and Planck functions of a range of temperatures (since the carrier of the 21 μm feature is expected to have a range of thermal equilibrium temperatures in the 21 μm -feature-emitting shell). Indeed, we find that with $\lambda_p = 20.1 \mu\text{m}$, $\gamma = 1.85 \mu\text{m}$, and $T \approx 90$ K, the product of a Drude profile and a single-temperature blackbody $\kappa_{\text{abs}}(\lambda) B_\lambda(T)$ closely fits the observed 21 μm emission feature [see the inserted panel in Fig. 1(h)]. In this work, we take $\lambda_p = 20.1 \mu\text{m}$ and $\gamma = 2.2 \mu\text{m}$ in order to maximize the energy output in the 21 μm feature so as to minimize the dust abundance requirement.

Table 1. Stellar and circumstellar parameters of HD 56126.

Central star ¹				
d/kpc	T_{eff}/K	R_*/R_{\odot}	L_*/L_{\odot}	
2.4	7250	49.2	6054	
Dust shell ¹				
R_{in}/cm	R_{out}/cm	M_{H}/M_{\odot} ²		
4.5×10^{16}	9.3×10^{16}	$\sim 0.16\text{--}0.44$		
Abundance of relevant elements (X/H , ppm) ³				
Ti	S	Fe	C	O
0.013	4.07	3.24	447	468
Total emitted power in the 21 μm band $E_{\text{tot}}(\text{erg s}^{-1})$ ¹				
1.0×10^{36}				

¹Data taken from Hony et al. (2003). ²Mass of the circumstellar shell depending on the assumed gas-to-dust ratio. ³Data taken from Van Winckel & Reyniers (2000).

HD 56126 (IRAS 07134+1005) is selected for the following reasons: (1) it is the strongest 21 μm feature emitter and its emission flux was accurately measured; (2) it is one of the best studied 21 μm feature sources and its basic parameters are accurately determined. Hony et al. (2003) built a detailed dust radiative transfer model for the circumstellar envelope and derived the composition and mass of the dust shell of HD 56126. Van Winckel & Reyniers (2000) performed a homogeneous photospheric abundance analysis of HD 56126 (as well as several other 21 μm feature sources). We summarize in Table 1 the key relevant stellar and circumstellar parameters which will be used in later analysis. The parameter M_{H} is not very certain in the range $\sim 0.16\text{--}0.44 M_{\odot}$. We generously take the high end ($M_{\text{H}} \approx 0.44 M_{\odot}$) for our analysis. Since the required minimum abundance $[X/H]_{\text{min}}$ is inversely proportional to M_{H} (see equation 5), if a model based on the high end $M_{\text{H}} \approx 0.44 M_{\odot}$ already exceeds the elemental budget it should certainly be rejected.

By assuming that the X atoms available in the circumstellar envelopes around the 21 μm feature sources (i.e. $[X/H]_*$) are *all* depleted in the dust species proposed as a carrier candidate, we obtain the *maximum* dust mass (relative to H) of the dust species containing the key element X from equation (2)

$$(M_{\text{d}}/M_{\text{H}})_{\text{max}} = \mu_{\text{d}} [X/H]_*/n_{\text{X}}. \quad (7)$$

This is the *upper* limit on the amount of dust containing element X *available* to account for the 21 μm feature. For a given dust temperature T_{d} , from equation 5, we obtain the *lower* limit on the amount of dust (relative to H) *required* to account for the 21 μm feature

$$(M_{\text{d}}/M_{\text{H}})_{\text{min}} = \mu_{\text{d}} [X/H]_{\text{min}}/n_{\text{X}} \\ = \frac{E_{\text{tot}}}{8\gamma \kappa_{\text{abs}}^{\text{int}} \int_{21 \mu\text{m band}} \{ [B_{\lambda}(T_{\text{d}})] / [(\lambda - \lambda_{\text{p}}^2/\lambda)^2 + \gamma^2] \} d\lambda}. \quad (8)$$

Apparently, for a valid carrier candidate, the minimum required mass $(M_{\text{d}}/M_{\text{H}})_{\text{min}}$ should not exceed the maximum available mass $(M_{\text{d}}/M_{\text{H}})_{\text{max}}$.

In Fig. 2, we plot $(M_{\text{d}}/M_{\text{H}})_{\text{max}}$ against $\kappa_{\text{abs}}^{\text{int}}$ for the proposed carrier candidates. We also plot $(M_{\text{d}}/M_{\text{H}})_{\text{min}}$ as a function of $\kappa_{\text{abs}}^{\text{int}}$ for a range of temperatures T_{d} . Note that the temperature at which $(M_{\text{d}}/M_{\text{H}})_{\text{max}} \approx (M_{\text{d}}/M_{\text{H}})_{\text{min}}$ is the *lowest* temperature the dust should have. For example, at $T \approx 880$ K, TiC nanoclusters have $(M_{\text{d}}/M_{\text{H}})_{\text{max}} \approx (M_{\text{d}}/M_{\text{H}})_{\text{min}}$. In order for $(M_{\text{d}}/M_{\text{H}})_{\text{min}}$ not exceeding $(M_{\text{d}}/M_{\text{H}})_{\text{max}}$, TiC dust must have $T_{\text{d}} > 880$ K, otherwise there is simply not enough dust material.

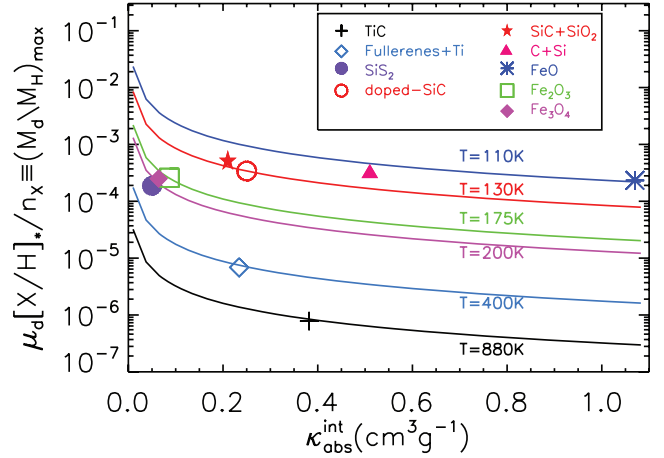


Figure 2. $\kappa_{\text{abs}}^{\text{int}}$, the integrated mass absorption coefficient of the 21 μm band (with the continuum underneath the band subtracted) versus $(M_{\text{d}}/M_{\text{H}})_{\text{max}} \equiv \mu_{\text{d}} [X/H]_*/n_{\text{X}}$, the maximum dust mass (relative to H) of the species containing the key element ‘X’ (obtained by assuming that all X atoms are tied in that particular dust species), as denoted by cross (TiC nanoclusters), open diamond (fullerenes coordinated with Ti atoms), filled circle (SiS_2), open circle (doped-SiC), filled star (SiO_2 -coated SiC), filled triangle (carbon-silicon mixtures), asterisk (FeO), open square (Fe_2O_3) and filled diamond (Fe_3O_4). Also plotted (as solid lines) are the minimum dust mass required to account for the emitted power of the 21 μm feature $(M_{\text{d}}/M_{\text{H}})_{\text{min}} \equiv \mu_{\text{d}} [X/H]_{\text{min}}/n_{\text{X}}$ as a function of $\kappa_{\text{abs}}^{\text{int}}$ for a range of temperatures.

4 ASSESSING INDIVIDUAL CARRIER CANDIDATES

We assess proposed individual carrier candidates by examining (1) whether they are capable of emitting the observed large amount of energy in the 21 μm band without requiring more dust material than available, and (2) whether the candidate carrier produces (undetected) secondary features. In view of the crucial role of elemental abundances in this assessment, we divide the carrier candidates into four groups: titanium-bearing, sulphur-bearing, silicon-bearing and iron-bearing grains.

The 3.3, 7.7 and 11.3 μm PAH features and the much more prominent 30 μm feature which is generally attributed to MgS dust (Goebel & Moseley 1985; Hony, Waters & Tielens 2002) are seen in 14 of 16 known 21 μm feature sources (Kwok et al. 1999; Hrivnak et al. 2009). Except these features, the 21 μm sources do not universally show any additional dust features. However, in addition to the 21 μm feature, some of the proposed carrier candidates exhibit strong spectral features at other wavelengths as well which are not detected at all or very weak in the 21 μm sources.

In view of the wide detection of the PAH features (and some flat plateau attributed to HAC) and the 30 μm feature in the 21 μm sources, Buss et al. (1993) suggested that the 21 μm feature might originate from some organic molecules like PAHs, while Goebel (1993) argued that sulphide could be the carrier candidate. But the proposition of a carrier candidate based on its matching to these accompanying features is potentially problematic since they vary from source to source, while the profile of the 21 μm feature is rather universal (i.e. with the same peak wavelength, a very similar FWHM and asymmetrical shape with a long red tail) indicating that the carrier of this feature should be the same in different sources. We also note that observationally, there does not appear to show any correlation between the strength of the 21 μm feature with that of the 30 μm feature (Jiang, Zhang & Li 2009).

For a given proposed carrier, the predicted intensity ratios of the associated features to the primary 21 μm feature must either be compatible with that observed (in case of detection) or not exceed the upper limit (in case of non-detection). SiC dust with carbon impurities, once considered as a promising candidate due to its abundant occurrence (Speck & Hofmeister 2004), was challenged based on the much higher model-predicted intensity ratio of the 11.3 μm feature to the 21 μm feature than observed (Jiang, Zhang & Li 2005).

4.1 Titanium-bearing grains

Titanium is a relatively rare element in the Solar system ($[\text{Ti}/\text{H}]_{\odot} \approx 9.77 \times 10^{-8}$; Grevesse 1989), and the Ti abundance in the metal-poor star HD 56126 is even lower: $[\text{Ti}/\text{H}] \approx 1.3 \times 10^{-8}$ (Van Winckel & Reyniers 2000). Although some Ti-bearing grains (e.g. TiC nanoclusters and fullerenes coordinated with Ti atoms) have a 21 μm feature with a close similarity to the 21 μm feature observed in PPNe, the deficiency of titanium would be a potential problem.

4.1.1 Titanium carbide

Von Helden et al. (2000) argued that the 21 μm feature may arise from titanium carbide nanoclusters (made of 27 to 125 atoms). The laboratory-measured spectral profiles of TiC nanoclusters match almost perfectly with the intrinsic profile of the observed 21 μm feature, better than any other candidate materials, although bulk TiC dust does not display a strong 21 μm band (see Henning & Mutschke 2001; Kimura & Kaito 2003b). The TiC hypothesis gains its strength from the identification of pre-solar TiC grains (with radii ~ 100 Å) in primitive meteorites as nanometre-sized inclusions embedded in micrometer-sized pre-solar graphite grains (Bernatowicz et al. 1996). However, since Ti is a rare element, the abundance test would be a neck to the TiC hypothesis. Indeed, three different groups have already challenged the TiC hypothesis from the Ti abundance point of view (Chigai et al. 2003; Hony et al. 2003; Li 2003). They all pointed out that there may not be enough titanium to account for the observed strength of this feature. Here, we add another piece of evidence against the TiC hypothesis by confronting it with the band-strength constraint discussed in Section 2. Unlike previous studies, in this approach, we do not need to know the ultraviolet/optical absorption properties of TiC. The experimental IR absorption spectrum of TiC nanoclusters was measured (Von Helden et al. 2000) and fitted with a Lorentz oscillator model (Chigai et al. 2003). The observational emission spectrum of HD 56126 and the experimental Lorentz profile of the 21 μm band are shown in Fig. 1(a).

The integrated mass absorption coefficient of nano TiC is $\kappa_{\text{abs}}^{\text{int}} \approx 0.38 \text{ cm}^3 \text{ g}^{-1}$ for the 21 μm band, as derived from the experimental spectrum of Von Helden et al. (2000). The emission temperature associated with the 21 μm carrier is not well constrained.

Exposed to the stellar radiation, TiC nanocrystals, because of their small heat capacities, will not attain an equilibrium temperature; instead, they will be transiently heated by single photons (see Draine & Li 2001). The stellar atmospheric spectrum of HD 56126 peaks at $\lambda \approx 0.41 \mu\text{m}$, i.e. a typical stellar photon has an energy of $\langle h\nu \rangle \approx 3 \text{ eV}$. With a Debye temperature of $\Theta \approx 614 \text{ K}$ (Pierson 1996), when heated by a 3 eV photon, for a TiC nanocluster as small as $\text{Ti}_{14}\text{C}_{13}$ (consisting of $3 \times 3 \times 3$ atoms) the peak temperature is only $T_{\text{peak}} \approx 268 \text{ K}$.

We calculate from equation (5) the minimum abundance requirement of $\text{Ti}_{14}\text{C}_{13}$ dust to be $[\text{Ti}/\text{H}]_{\text{min}} \approx 1.97 \times 10^{-7}$ at $T_{\text{d}} = 268 \text{ K}$. Since the titanium abundance in HD 56126 is measured to be $[\text{Ti}/\text{H}]_{\star} \approx 1.3 \times 10^{-8}$ (see Table 1), the minimum abundance requirement (at $T_{\text{d}} = 268 \text{ K}$) exceeds the available abundance by a factor of ~ 15 .

For a given exciting photon energy (say, $h\nu = 3 \text{ eV}$), the peak temperature decreases with the nanocluster size: $T_{\text{peak}} \approx 216 \text{ K}$ for $\text{Ti}_{32}\text{C}_{32}$ (consisting of $4 \times 4 \times 4$ atoms) and $T_{\text{peak}} \approx 183 \text{ K}$ for $\text{Ti}_{72}\text{C}_{53}$ (consisting of $5 \times 5 \times 5$ atoms). Therefore, larger TiC nanoclusters would require even more Ti atoms to account for the observed 21 μm intensity.

In fact, based on the available Ti abundance in HD 56126, nano TiC grains have to reach a temperature at least as high as $\sim 880 \text{ K}$ to achieve the observed emission strength [i.e. $(M_{\text{d}}/M_{\text{H}})_{\text{min}} \approx (M_{\text{d}}/M_{\text{H}})_{\text{max}}$; see Fig. 2], while the peak temperature is only $\sim 268 \text{ K}$ even for a small cluster consisting of only 27 atoms. Apparently, the TiC hypothesis requires too much Ti to be viable, even under the most optimal condition that all Ti atoms are locked in TiC nanocrystals.

4.1.2 Fullerenes coordinated with Ti atoms

Kimura et al. (2005) found that the laboratory spectra of large-cage carbon particles (fullerenes) coordinated with Ti atoms have a characteristic feature at $\sim 20.3 \mu\text{m}$ closely resembling the 21 μm feature of post-AGB stars [see Fig. 1(b)]. They attributed the origin of the 21 μm feature to the vibrational interaction between Ti atoms and fullerene cages. In order to obtain the integrated mass absorption coefficient $\kappa_{\text{abs}}^{\text{int}}$ only over the 21 μm band, the continuum absorption needs to be subtracted. Based on the continuum spectrum between 15–18.5 and 22–24 μm , we use a two-order polynomial to fit the continuum underneath the 21 μm feature. In the following sections, unless otherwise stated, the continuum absorption is determined in the same way. The resulting continuum-subtracted, integrated mass absorption coefficient for the 21 μm is $\kappa_{\text{abs}}^{\text{int}} \approx 0.233 \text{ cm}^3 \text{ g}^{-1}$.

Similar to TiC nanoclusters, fullerenes will also subject to stochastic heating in the circumstellar envelope around HD 56126. With a Debye temperature of $\Theta \approx 185 \text{ K}$,² when heated by a typical photon of 3 eV in HD 56126, even C_{60} is only heated to a peak temperature of $T_{\text{peak}} \approx 89 \text{ K}$.³

With $\kappa_{\text{abs}}^{\text{int}} \approx 0.233 \text{ cm}^3 \text{ g}^{-1}$ and $T_{\text{peak}} \approx 89 \text{ K}$, from equation (5), we estimate the minimum abundance requirement of fullerenes with Ti atoms to be $[\text{Ti}/\text{H}]_{\text{min}} \approx 8.04 \times 10^{-6}$, exceeding the available Ti abundance $[\text{Ti}/\text{H}]_{\star} \approx 1.3 \times 10^{-8}$ by a factor of ~ 618 . In order not to violate the abundance constraint (i.e. $[\text{Ti}/\text{H}]_{\text{min}} < [\text{Ti}/\text{H}]_{\star}$, or $(M_{\text{d}}/M_{\text{H}})_{\text{min}} < (M_{\text{d}}/M_{\text{H}})_{\text{max}}$), the dust temperature should be higher than 400 K (see Fig. 2), while the peak temperature of the $\text{C}_{60} + \text{Ti}$ dust is only $\sim 89 \text{ K}$. Therefore, large fullerenes coordinated with Ti atoms are unlikely the carrier of the 21 μm feature seen in PPNe.

4.2 Sulphur-bearing grains: silicon disulfide

The formation of sulphide is very likely to occur in carbon-rich circumstellar environments. As early as 30 yr ago, Lattimer, Schramm

² See <http://www.sesres.com/PhysicalProperties.asp>.

³ For larger fullerenes, we expect a lower peak temperature T_{peak} and therefore require a higher minimum abundance $[\text{Ti}/\text{H}]_{\text{min}}$, indicating a more severe Ti abundance budget shortage.

& Grossman (1978) predicted the possible presence of various sulphur-bearing materials in carbon-rich systems. For several kinds of predicted sulphides, including MgS, FeS, SiS₂ and CaS, the absorption spectra and coefficients have been measured in laboratory (Nuth et al. 1985). The prominent 30 μm dust feature seen in AGB, post-AGB and PNe, amounting to more than 20 per cent of the total IR flux, is attributed to MgS (Goebel & Moseley 1985; Hony et al. 2002). Since most of the 21 μm sources also exhibit a strong feature at 30 μm , it is not unreasonable to postulate that some sulphur-bearing grains may also contribute to the 21 μm feature. Indeed, the laboratory spectrum of SiS₂ displays a prominent feature at ~ 22 μm (Nuth et al. 1985). Goebel (1993) further suggested SiS₂ solids as the material responsible for the 21 μm feature.

Based on the laboratory spectra of Goebel (1993) and Nuth et al. (1985), we obtain $\kappa_{\text{abs}}^{\text{int}} \approx 0.05 \text{ cm}^3 \text{ g}^{-1}$ for the 21 μm band of SiS₂ after subtracting the continuum (see Fig. 1). In addition to the 21 μm band, the laboratory absorption spectrum of SiS₂ also exhibits a secondary feature at 17 μm that is never observed in the 21 μm sources (Kraus, Nuth & Nelson 1997). In order to sufficiently suppress the 17 μm feature so that it remains un-notable, the dust temperature needs to be < 100 K. For $T_{\text{d}} = 100$ K we estimate the minimum abundance requirement of SiS₂ to be $[S/H]_{\text{min}} \approx 9.59 \times 10^{-5}$, exceeding the available S abundance $[S/H]_{\star} \approx 4.07 \times 10^{-6}$ by a factor of ~ 24 . As shown in Fig. 2, in order for the SiS₂ model to satisfy the abundance constraint (i.e. $[S/H]_{\text{min}} < [S/H]_{\star}$ or $(M_{\text{d}}/M_{\text{H}})_{\text{min}} < (M_{\text{d}}/M_{\text{H}})_{\text{max}}$), SiS₂ dust needs to be hotter than ~ 200 K.

Posch et al. (2004) also recognized that very low dust temperatures (significantly lower than 100 K) would be required to make the secondary feature at 17 μm negligible in strength compared to the 21 μm SiS₂ feature. Although it is not possible to calculate the equilibrium temperature of SiS₂ due to the lack of knowledge of its visual and near-IR optical constants, Posch et al. (2004) argued that ‘it is hardly conceivable that SiS₂ is so transparent in the visual range as to remain much colder than 100 K’. In our approach, we actually do not need to know the exact temperature of SiS₂: (1) if $T < 100$ K – although the 17 μm feature will be suppressed, one requires too much S; (2) if $T > 200$ K – although there will not be a S-budget problem, the 17 μm feature will be prominent. Therefore, our approach readily ruled out SiS₂.

Moreover, it is worth noting that sulphur may not be completely locked in SiS₂. The prominent 30 μm feature, if indeed arising from MgS, would consume a significant portion of the sulphur available in the circumstellar envelopes around the 21 μm sources. According to Zhukovska & Gail (2008), MgS has priority in the cooling sequence of sulphur-bearing solid compound.

4.3 Silicon-bearing grains

With four valence electrons, Si easily reacts with other atoms such as C, O, Fe and Mg to form various types of silicates. In the O-rich dust shells of evolved stars (from AGB stars to PNe), both amorphous and crystalline silicates are detected through their numerous emission bands. Over 4000 sources are detected to have the most common silicate features at 9.7 and 18 μm . While in the C-rich dust shells like those of the 21 μm sources, relatively simple Si-bearing compounds are formed (e.g. SiC, SiO₂ and SiS₂). The broad 11.3 μm feature seen in five of the sixteen 21 μm sources (Kwok et al. 1999) is identified to arise from the Si–C stretching mode of SiC. Being chemically active and abundant in circumstellar envelopes, several Si-bearing dust species have been proposed to be the carrier of the 21 μm feature.

Silicon is an abundant element in the Universe (its solar abundance is $[\text{Si}/\text{H}]_{\odot} \approx 3.55 \times 10^{-5}$; Grevesse 1989), about one order of magnitude higher than sulphur. Unfortunately, the Si abundance $[\text{Si}/\text{H}]_{\star}$ has not been measured for our tester HD 56126. We take the following approach to roughly estimate $[\text{Si}/\text{H}]_{\star}$ of HD 56126. (1) We compile the abundance data of all 21 μm sources and find that five 21 μm sources – IRAS 04296, IRAS 22223, IRAS 23304, (Van Winckel & Reyniers 2000) and IRAS 05113, IRAS 22272 (Reddy et al. 2002) – have known Si abundance. (2) We calculate the abundance ratios of Si to Ca and of Si to S for all five sources and find that these ratios do not vary much.⁴ (3) By assuming that the Si to Ca and Si to S abundance ratios of HD 56126 are similar to that of the other five 21 μm sources, we estimate $[\text{Si}/\text{H}]_{\star} \approx 6.31$ ppm for HD 56126 from $\{\text{Si}/\text{Ca}\} \approx 1.55$ and $[\text{Ca}/\text{H}]_{\star} \approx 0.18$ ppm (Van Winckel & Reyniers 2000) or $[\text{Si}/\text{H}]_{\star} \approx 10.7$ ppm from $\{\text{Si}/\text{S}\} \approx 0.42$ and $[\text{S}/\text{H}]_{\star} \approx 4.07$ ppm. (4) We finally take the Si abundance of HD 56126 to be the average of that estimated from Ca and S, $[\text{Si}/\text{H}]_{\star} \approx 8.5$ ppm.

4.3.1 Doped-SiC

Silicon carbide (SiC) grains with impurities were suggested to be the carrier of the 21 μm feature, based on laboratory data that doped SiC grains exhibit a resonance at ~ 21 μm (Speck & Hofmeister 2004). This proposal gains strength from the fact that SiC is a common dust species in carbon-rich circumstellar envelopes. The presence of circumstellar SiC grains was first revealed by Gilra (1972). Nowadays, SiC is believed to be the contributor of the well-known IR dust feature at 11.3 μm observed in more than 700 carbon stars (Kwok, Volk & Bidelman 1997). Since five of the sixteen 21 μm sources (i.e. about 40 per cent) exhibit the 11.3 μm feature, it is not unreasonable to consider both features coming from the same carrier. In particular, the distributions of the dust emitting at 21 and 11.3 μm are co-spatial in two 21 μm sources (HD 56126 and IRAS Z02229+6208; Kwok et al. 2002), which also supports the SiC hypothesis as the 21 μm carrier.

However, the 21 μm feature is *secondary* and much weaker than the *primary* 11.3 μm feature in the experimental spectrum of SiC (Speck & Hofmeister 2004). Jiang et al. (2005) assumed a single Lorentz oscillator model for the 21 μm feature with $Q_{\text{abs}}(21 \mu\text{m})/a$ treated as a free parameter [where $Q_{\text{abs}}(\lambda)$ is the absorption efficiency at wavelength λ and a is the dust size]. They found that the predicted 11.3 μm feature is still much stronger than observed even with $Q_{\text{abs}}(21 \mu\text{m})/a = 10^4 \text{ cm}^{-1}$. It is unlikely to expect the strength of the 21 μm feature, a secondary feature of SiC caused by impurities, would be much stronger than that of the primary 11.3 μm feature for which $Q_{\text{abs}}(11.3 \mu\text{m})/a \approx 1.5 \times 10^4 \text{ cm}^{-4}$ (Jiang et al. 2005). Therefore, doped-SiC cannot produce the 21 μm feature without producing too strong a 11.3 μm feature to be consistent with observations.

Jiang et al. (2005) calculated the equilibrium temperatures and κ_{abs} of doped-SiC of different grain sizes and a range of

⁴ This may not be unexpected since S, Si and Ca all are α elements. Let $\{X/H\} \equiv \log_{10} [X/H] + 12$ and $\{X/Y\} \equiv \{X/H\} - \{Y/H\}$. For IRAS 04296, IRAS 22223, IRAS 23304, IRAS 05113 and IRAS 22272, the Si to Ca abundance ratios are, respectively, $\{\text{Si}/\text{Ca}\} \approx 1.80, 1.57, 1.69, 1.45$ and 1.49, with a mean ratio of $\{\{\text{Si}/\text{Ca}\}\} \approx 1.55$ (and a standard deviation of $\sigma \approx 0.12$). The Si to S abundance ratios vary a bit more compared to $\{\text{Si}/\text{Ca}\}$; they are, respectively, $\{\text{Si}/\text{S}\} \approx 0.70, 0.59, 0.57, 0.22$ and 0.28 for IRAS 04296, IRAS 22223, IRAS 23304, IRAS 05113 and IRAS 22272, with a mean ratio of $\{\{\text{Si}/\text{S}\}\} \approx 0.42$ (and a standard deviation of $\sigma \approx 0.18$).

$Q_{\text{abs}}(21\ \mu\text{m})/a$ values. For α -SiC, the equilibrium temperature is in a narrow range (~ 60 – 80 K), insensitive to the assumed $Q_{\text{abs}}(21\ \mu\text{m})/a$ values (see fig. 2 of Jiang et al. 2005). We see that even with $Q_{\text{abs}}(21\ \mu\text{m})/a = 10^4\ \text{cm}^{-1}$ (which implies $\kappa_{\text{abs}}^{\text{int}} \approx 0.25\ \text{cm}^3\ \text{g}^{-1}$), the required Si abundance is at least $\sim 8.76 \times 10^{-4}$ (for $T \approx 80$ K) and $\sim 2.31 \times 10^{-3}$ (for $T \approx 60$ K), way too much compared with $[\text{Si}/\text{H}]_{\star} \approx 8.5$ ppm estimated for HD 56126.

Unlike α -SiC, the equilibrium temperatures of β -SiC are sensitive to $Q_{\text{abs}}(21\ \mu\text{m})/a$ and become much higher for smaller $Q_{\text{abs}}(21\ \mu\text{m})/a$ (see fig. 3 of Jiang et al. 2005). We will consider cases with both large and small $Q_{\text{abs}}(21\ \mu\text{m})/a$. For $Q_{\text{abs}}(21\ \mu\text{m})/a = 100\ \text{cm}^{-1}$ (i.e. $\kappa_{\text{abs}}^{\text{int}} \approx 0.003\ \text{cm}^3\ \text{g}^{-1}$), submicron-sized β -SiC dust has an equilibrium temperature ~ 100 K (see fig. 3 of Jiang et al. 2005), suggesting that one requires at least $[\text{Si}/\text{H}]_{\text{min}} \approx 3.33 \times 10^{-3}$. For $Q_{\text{abs}}(21\ \mu\text{m})/a = 10^4\ \text{cm}^{-1}$ (i.e. $\kappa_{\text{abs}}^{\text{int}} \approx 0.28\ \text{cm}^3\ \text{g}^{-1}$), with a typical equilibrium temperature ~ 60 K (see fig. 3 of Jiang et al. 2005), the minimum required Si abundance is $[\text{Si}/\text{H}]_{\text{min}} \approx 3.80 \times 10^{-3}$. Therefore, for both α -SiC and β -SiC, one needs way too much Si, exceeding the Si abundance available in HD 56126 (~ 8.5 ppm) by two orders of magnitude. So it is secure to conclude that doped-SiC cannot be the carrier of the 21 μm feature.

4.3.2 SiC Core-SiO₂ mantle grains

Clément et al. (2003) carried out laboratory experiments and found that pure SiC nano-particles can be quite easily oxidized at their surfaces to form SiO₂-coated SiC grains. The oxidation can even reach a considerable volume fraction of the particles. The laboratory spectra of the partially oxidized SiC grains show an absorption feature at ~ 21 – $22\ \mu\text{m}$. Posch et al. (2004) suggested that dust composed of a SiC core and a SiO₂ mantle may be the carrier of the 21 μm feature.

From the $Q_{\text{abs}}(\lambda)/a$ values of Posch et al. (2004), we obtain $\kappa_{\text{abs}}^{\text{int}} \approx 0.21\ \text{cm}^3\ \text{g}^{-1}$. The equilibrium temperatures of submicron-sized SiC core-SiO₂ mantle grains is ~ 104 – 126 K in the 21 μm emitting region of HD 56126 (Posch et al. 2004). The minimum requirement of Si is $\sim 1.00 \times 10^{-5}$ – 3.22×10^{-5} , which is slightly above the available Si abundance of $[\text{Si}/\text{H}]_{\star} \approx 8.50$ ppm.

However, these core-mantle grains have two prominent features [see Fig. 1(d)] at 8.3 μm (arising from the SiO₂ mantle) and 11.3 μm (arising from the SiC core). The 8.3 μm feature is never seen in the 21 μm sources except three 21 μm sources appear to have a plateau at $\sim 8\ \mu\text{m}$ with an average FWHM of $\sim 4\ \mu\text{m}$ which is more likely from HAC or the C–C stretching mode of PAHs (Kwok, Volk & Bernath 2001). As far as the 11.3 μm feature is concerned, we compare the flux ratio of the 11.3 μm band to the 21 μm band observed in HD 56126 [$F(11.3\ \mu\text{m})/F(21\ \mu\text{m}) < 0.012$] (Hony et al. 2003) with that predicted from the SiC core-SiO₂ mantle model. It is found that the dust should be colder than ~ 70 K in order not to produce too strong a 11.3 μm feature. However, the equilibrium temperature of submicron-sized SiC core-SiO₂ mantle grains is ~ 104 – 126 K in the 21 μm emitting region of HD 56126 (Posch et al. 2004). Moreover, if the dust temperature is as low as < 70 K, the minimum Si abundance requirement would be $\sim 8.05 \times 10^{-4}$, exceeding the Si abundance available in HD 56126 ($[\text{Si}/\text{H}]_{\star} \approx 8.50$ ppm) by a factor of ~ 10 .

In addition, the opacity profile of these grains has a shoulder in the red-wing of the 21 μm band which is not observed in the 21 μm sources. Therefore, both the secondary features and the 21 μm pro-

file are discrepant with observations, suggesting that SiC core-SiO₂ mantle grains are not a valid carrier candidate.

4.3.3 Solid-solution phase of carbon and silicon with a diamond structure

Kimura et al. (2005) measured the IR absorption spectra of silicon-containing carbon films prepared by ion sputtering of carbon and silicon carbide mixture pellets. The carbon-silicon mixture film, composed of a solid-solution phase of carbon and silicon with a diamond structure, show significant absorption features at 9.5 and 21 μm [see Fig. 1(e)]. Thus, Kimura et al. (2005) suggested that the 21 μm feature observed in PPNe may arise from the solid-solution phase of carbon and silicon with a diamond structure.

However, the 9.5 μm feature is far stronger than the 21 μm feature in the carbon-silicon mixture film, but it is never seen in the 21 μm sources. In order to suppress the 9.5 μm feature to such a level that the total flux emitted in the 9.5 μm band is less than, say 10 per cent of that in the 21 μm feature, the critical dust temperature, depending on the silicon percentage, needs to be < 102 K for C–30 per cent Si film or < 120 K for C–10 per cent Si film.

Unfortunately, there lacks a full knowledge of the optical properties of such carbon-silicon mixtures to determine their equilibrium temperatures. We adopt the dielectric functions of diamonds which may be a reasonable approximation of the carbon-silicon mixtures with a diamond structure (Kimura & Kaito 2003a). We find the temperature of submicron-sized diamonds in the 21 μm -emitting region of HD 56126 is ~ 148 – 182 K.⁵ Therefore, the carbon-silicon mixtures, if they are indeed responsible for the 21 μm feature, would produce too strong a 9.5 μm emission feature to be consistent with that observed in the 21 μm feature sources.

4.4 Iron-bearing grains

4.4.1 Fe₂O₃ and Fe₃O₄

Iron oxides were first suggested as the carrier of the 21 μm feature by Cox (1990). Cox (1990) reported the detection of a 21 μm emission feature in the IRAS LRS spectra of 10 H II regions and associated it with the 21 μm band seen in PPNe. From the strength and the ‘universality’ of this feature in H II regions, iron oxides γ -Fe₂O₃ (maghemite) and Fe₃O₄ (magnetite) were assigned to this band. However, Oudmaijer & de Winter (1995) later re-analysed the IRAS LRS spectra of these sources and concluded that the claimed 21 μm band was just an artefact. This was confirmed in late 1990s when some of these H II regions were observed with ISO which show no footprints of a broad 21 or 20 μm band (Posch et al. 2004). In fact, the laboratory absorption spectra of iron oxides of Cox (1990) were quite different from the intrinsic profile of the 21 μm feature of PPNe which had not been well identified until Volk, Kwok & Hrivnak (1999). But of course the spectral profile match might be improved if one considers dust shape and clustering effects. Therefore, iron oxides are not readily ruled out just based on the imperfect spectral match.

⁵ The Si abundance is less of an issue. From the absorption profiles of Kimura et al. (2005), we obtain $\kappa_{\text{abs}}^{\text{int}} \approx 0.32\ \text{cm}^3\ \text{g}^{-1}$ for C–50 per cent Si film, $0.51\ \text{cm}^3\ \text{g}^{-1}$ for C–30 per cent Si film and $0.40\ \text{cm}^3\ \text{g}^{-1}$ for C–10 per cent Si film. If the dust temperature is, respectively, higher than ~ 130 , ~ 110 and ~ 100 K for C–50 per cent Si film, C–30 per cent Si film and C–10 per cent Si film, the minimum required Si abundance would not exceed that available in HD 56126.

Despite that the 21 μm feature found in H II regions turns out to be an artefact, iron oxides composed of cosmically abundant elements and exhibiting a strong feature around 20 μm deserve a detailed study as being the carrier of the 21 μm feature seen in PPNe. In addition to $\gamma\text{-Fe}_2\text{O}_3$, other forms of Fe_2O_3 exhibit a feature around 21 μm as well. Koike et al. (1981) indicated hematite ($\alpha\text{-Fe}_2\text{O}_3$) has several peaks at $\sim 9.2, 18, 21$ and $30 \mu\text{m}$ in its absorption spectrum. Similarly, the absorption spectrum of Fe_3O_4 shows two features at ~ 17 and $25 \mu\text{m}$.

Cox (1990) only presented the normalized absorption profiles of two iron oxides ($\gamma\text{-Fe}_2\text{O}_3$ and Fe_3O_4), which cannot be used to calculate $\kappa_{\text{abs}}^{\text{int}}$. Based on the unpublished optical constants of Fe_2O_3 and Fe_3O_4 from the Jena group,⁶ $\kappa_{\text{abs}}(\lambda)$ and $\kappa_{\text{abs}}^{\text{int}}$ are calculated from Mie theory and assuming a spherical radius of 0.1 μm . We obtain $\kappa_{\text{abs}}^{\text{int}} \approx 0.09 \text{ cm}^3 \text{ g}^{-1}$ for Fe_2O_3 and $0.07 \text{ cm}^3 \text{ g}^{-1}$ for Fe_3O_4 . As shown in Figs 1(f) and (g), Fe_2O_3 displays two strong bands at $\sim 20.5 \mu\text{m}$ and $27.5 \mu\text{m}$, while Fe_3O_4 exhibits two broad features at $\sim 16.5 \mu\text{m}$ and $24 \mu\text{m}$. Apparently, Fe_3O_4 does not fit the 21 μm feature seen in PPNe – the model feature peak is neither strong nor at the right wavelength [see Fig. 1(g)]. For Fe_2O_3 , even with temperature fine-tuning, it is very hard to suppress the 27.5 μm feature which is not seen in the 21 μm sources.

Moreover, Fe_2O_3 and Fe_3O_4 may not be able to survive in such a reducing environment like C-rich circumstellar envelopes of the 21 μm sources (Posch et al. 2004). Therefore, Fe_2O_3 and Fe_3O_4 are unlikely responsible for the 21 μm feature seen in PPNe.

4.4.2 FeO

Posch et al. (2004) pointed out that iron monoxide (FeO; wüstite) can survive in the C-rich reducing environment and proposed that nano-sized FeO dust may be the carrier of the 21 μm feature seen in PPNe. FeO will be reduced to metal iron by UV photons in PNe, while it is less likely for oxygen to stick to iron to form FeO in AGB stars whose circumstellar dust is much hotter than in PPNe. Since FeO can be either oxygenated to higher oxides of iron or reduced to iron atoms, it can survive only in a very strict physical and chemical environment, which is consistent with the observational fact that the 21 μm band is rarely seen and detected only in PPNe that live for a short transitory period.

We adopt the dielectric functions of pure FeO measured by Henning & Mutschke (1997) at temperatures $T = 10, 100, 200$ and 300 K to calculate the absorption spectrum of FeO dust. It is found that FWHM of the 21 μm band of FeO decreases from $\sim 3.6 \mu\text{m}$ at room temperature to $\sim 2.4 \mu\text{m}$ at $T = 100 \text{ K}$, while the band peak λ_{peak} shifts from ~ 19.9 to $\sim 20.1 \mu\text{m}$. At $T = 100 \text{ K}$, both FWHM and λ_{peak} of FeO agree well with the observed 21 μm profile.

Adopting the dielectric functions of FeO measured at $T = 100 \text{ K}$ and assuming spherical dust of radii $a = 1 \text{ nm}$ as suggested by Posch et al. (2004), we calculate $\kappa_{\text{abs}}^{\text{int}} \approx 1.07 \text{ cm}^3 \text{ g}^{-1}$ for FeO [Fig. 1(h) shows the calculated κ_{abs} profile which is closely reproduced by a Drude function with $\lambda_{\text{p}} = 20.1 \mu\text{m}$ and $\gamma = 2.4 \mu\text{m}$]. Nano-sized FeO grains will be stochastically heated by single stellar photons (see Draine & Li 2001). With a Debye temperature of $\Theta \approx 650 \text{ K}$ (Radwanski & Ropka 2008), the peak temperature of a 1 nm FeO dust is $T_{\text{peak}} \approx 143 \text{ K}$ when heated by a typical photon of 3 eV in HD 56126. At $T_{\text{d}} = 143 \text{ K}$ the minimum abundance requirement is $[\text{Fe}/\text{H}]_{\text{min}} \approx 5.76 \times 10^{-7}$. This is smaller than the stellar abundance $[\text{Fe}/\text{H}]_{\star} \approx 3.24 \times 10^{-6}$ (see Fig. 2). Note that HD 56126 is the most

iron-poor object among the sixteen 21 μm sources. Therefore, the FeO hypothesis will generally satisfy the abundance requirement.

FeO has no notable secondary features in the IR, except a small shoulder in the blue wing of the 21 μm band which is not seen in the 21 μm sources.

Stochastically heated FeO nano dust is expected to have a distribution of temperatures ($T < T_{\text{peak}} = 143 \text{ K}$). Although the optical properties of FeO change strongly with temperature, at $T < 100 \text{ K}$ they are much less sensitive to temperature (see Henning & Mutschke 1997). It is therefore reasonable to expect that FeO nano dust with a distribution of temperatures at $T < 143 \text{ K}$ also fits the observed 21 μm profile since the experimental spectrum of FeO obtained at $T = 100 \text{ K}$ provides the best match.

Finally, one may ask how FeO is formed in the C-rich shells around the 21 μm sources where it is generally believed that all O atoms are trapped in CO; or in other words, are there enough O atoms left to form FeO? Our answer is ‘yes’. The C and O abundances (relative to H) of HD 56126 are, respectively, $[\text{C}/\text{H}]_{\star} \approx 447 \text{ ppm}$ and $[\text{O}/\text{H}]_{\star} \approx 468 \text{ ppm}$ (Van Winckel & Reyniers 2000). A substantial fraction of the C atoms is required to be tied in the carbonaceous dust components (amorphous carbon [a-C] and HAC) to account for the bulk of the IR emission of HD 56126 (see Hony et al. 2003). Taking $M_{\text{a-c}} \approx 3.6 \times 10^{-4} M_{\odot}$ and $M_{\text{HAC}} \approx 3.6 \times 10^{-4} M_{\odot}$ for the mass of amorphous carbon and HAC in the dust shell around HD 56126 (Hony et al. 2003), we estimate the amounts of C atoms locked in amorphous carbon and HAC to be $[\text{C}/\text{H}]_{\text{a-c}} \approx 68 \text{ ppm}$ and $[\text{C}/\text{H}]_{\text{HAC}} \approx 65 \text{ ppm}$, respectively.⁷ Therefore, there will be at most $[\text{C}/\text{H}] \approx 314 \text{ ppm}$ C atoms in the gas phase to react with O. Assuming all gas-phase C atoms are tied with O atoms to form CO, there will be $[\text{O}/\text{H}] \approx 154 \text{ ppm}$ O atoms left for other O-containing molecules and dust species.⁸ Even assuming all Fe atoms are locked up in FeO dust, FeO only needs $[\text{O}/\text{H}] \approx 3.24 \text{ ppm}$ O atoms.

5 SUMMARY

We have quantitatively examined eight inorganic carrier candidates and one organic candidate for the 21 μm emission band detected in sixteen PPNe, by confronting the abundance and accompanying IR emission features required or predicted by each model with that observed. We take HD 56126, the strongest 21 μm feature source, as a testing case. The principal results of this paper are the following (see Table 2 for a summary).

(i) Among the nine carrier candidates, five (TiC nanoclusters, fullerenes coordinated with Ti atoms, SiS_2 , doped-SiC and SiO_2 -mantled SiC dust) are readily ruled out because they fall short of either titanium, sulphur, or silicon. Even under the most optimal

⁷ Here, we adopt $M_{\text{H}} \approx 0.44 M_{\odot}$, the high end of the H mass of the HD 56126 shell. If we adopt the low end of $M_{\text{H}} \approx 0.16 M_{\odot}$, the required C depletion in dust needs to be increased by a factor of ~ 2.8 . This implies that there will be fewer C atoms in the gas phase to form CO and therefore more O atoms will be available to form FeO. We take the molecular weight of HAC to be $\mu_{\text{HAC}} \approx 12.5 \mu_{\text{H}}$ (with $\text{H}/(\text{H} + \text{C}) \approx 0.35$, Hony et al. 2003).

⁸ Duley (1980) showed that the oxidation of metallic iron is a very efficient process provided that enough O_2 molecules are present. FeO is a preferential product of low-temperature oxidation (e.g. see Roberts 1961; Fehlnner & Mott 1970, while Fe_2O_3 and Fe_3O_4 are more likely formed at higher temperatures (e.g. see Gail & Sedlmayr 1998). Posch et al. (2004) argued that the low-temperature oxidation of very small iron grains – grains composed of $< 10^3$ atoms with a size of $a \leq 1 \text{ nm}$ could result in pure FeO dust (instead of a large metallic iron core and a tiny FeO mantle).

⁶ <http://www.astro.uni-jena.de/Laboratory/OCDB/oxsul.html#B1>

Table 2. Tests of abundance and possible accompanying features for nine carrier candidates of the 21 μm feature seen in PPNe.

Candidate material	Element X	$\kappa_{\text{abs}}^{\text{int}}$ ($\text{cm}^3 \text{g}^{-1}$)	$[\text{X}/\text{H}]_{\text{min}}$ (ppm)	$[\text{X}/\text{H}]_{\star}$ (ppm)	Associated features	Pass (\checkmark) or Fail (\times)
Nano TiC	Ti	0.38	0.197 ($T = 268 \text{ K}$)	0.013	...	\times
Fullerenes + Ti	Ti	0.23	8.04 ($T = 89 \text{ K}$)	0.013	...	\times
SiS ₂	S	0.05	95.9 ($T = 100 \text{ K}$)	4.07	16.8 μm	\times
Doped-SiC	Si	0.25	876 ($T = 80 \text{ K}$)	8.50	11.3 μm	\times
SiC + SiO ₂	Si	0.21	805 ($T = 70 \text{ K}$)	8.50	8.3, 11.3 μm	\times
Si + C mixture	Si	9.5 μm	\times
Fe ₂ O ₃	Fe	0.09	3.05 ($T = 175 \text{ K}$)	3.24	9.2, 18, 27.5 μm	\times
Fe ₃ O ₄	Fe	0.06	2.92 ($T = 200 \text{ K}$)	3.24	16.5, 24 μm	\times
FeO	Fe	1.07	0.576 ($T = 143 \text{ K}$)	3.24	...	\checkmark

condition, the minimum Ti, S or Si abundance required to account for the observed 21 μm feature strength still substantially exceeds the available amount in the 21 μm sources.

(ii) Three candidates (carbon-silicon mixtures, Fe₃O₄ and Fe₂O₃) are ruled out because they produce strong secondary features (in addition to the 21 μm feature) which are not seen in the 21 μm feature sources.

(iii) FeO nano dust, closely matching the observed 21 μm emission feature neither exceeds the Fe abundance budget nor produces undetected secondary features. There are also plenty of O atoms in the dust shell around HD 56126 to form FeO, although it is a C-rich environment. Therefore, nano-sized FeO seems to be a viable candidate.

By taking an alternative approach based on abundance constraints complementary to that based on spectral profile matching, our results are consistent with that of Posch et al. (2004) except (1) we have also ruled out two newly suggested candidates (i.e. fullerenes coordinated with Ti atoms, carbon-silicon mixtures); (2) SiC core-SiO₂ mantle dust is more firmly ruled out as a valid candidate and (3) we provide further support to the FeO hypothesis of Posch et al. (2004). Our approach does not rely on detailed spectral profile fitting which could be largely affected by dust size, shape and clustering effects.

We have not applied the above tests to the organic candidates (i.e. urea or thiourea, PAHs and HAC) for three reasons: (1) the optical properties of urea or thiourea are not known; (2) although ten of the sixteen 21 μm sources show PAH emission features at the so-called 3.3, 6.2, 7.7, 8.2 and 11.3 μm ‘unidentified IR (UIR)’ bands, PAHs are unlikely a viable candidate since their 21 μm band strength is much weaker than that of the ‘UIR’ bands and (3) HAC is an ill-characterized material; its optical properties are sensitive to the H/C and sp²/sp³ ratios (see Jones, Duley & Williams 1990; Furton, Laiho & Witt 1999); its 21 μm band strength (especially relative to its vibrational bands at $\sim 6\text{--}8 \mu\text{m}$) is not well determined. To us, PAH clusters probably deserve a detailed investigation.

ACKNOWLEDGMENTS

We thank the anonymous referee for his/her very useful suggestions. BWJ and KZ are supported in part by China’s grants 2007CB815406, NSFC 10473003 and NCET-05-0144. AL is supported in part by Spitzer Theory Programs, the Spitzer Cycle 3 GO program P30403 and NSF grant AST 07-07866.

REFERENCES

- Andersen A. C., Posch T., Mutschke H., 2005, in Wilson A., ed., ESA SP-577, Pitfalls in the Identification of the 21 Micron Feature. ESA, Noordwijk, p. 447
- Bernatowicz T., Cowsik R., Gibbons Patrick C., Lodders K., Fegley Bruce J., Amari S., Lewis R. S., 1996, ApJ, 472, 760
- Buss R. H. Jr., Tielens A. G. G. M., Cohen M., Werner M. W., Bregman J. D., Witteborn F. C., 1993, ApJ, 415, 250
- Chigai T., Yamamoto T., Kaito C., Kimura Y., 2003, ApJ, 587, 771
- Clément D., Mutschke H., Klein R., Henning T., 2003, ApJ, 594, 642
- Cox P., 1990, A&A, 236, L29
- Draine B. T., Li A., 2001, ApJ, 551, 807
- Duley W. W., 1980, ApJ, 240, 950
- Fehlner F. P., Mott N. F., 1970, Oxid. Met., 2, 59
- Furton D. G., Laiho J. W., Witt A. N., 1999, ApJ, 526, 752
- Gail H.-P., Sedlmayr E., 1998, Chemistry and Physics of Molecules and Grains in Space. Faraday Discussions No. 109 Inorganic dust formation in astrophysical environments. The Faraday Division of the Royal Society of Chemistry, London, p. 303
- Gilra D. P., 1972, PhD thesis, Univ. Wisconsin-Madison
- Goebel J. H., 1993, A&A, 278, 226
- Goebel J. H., Moseley S. H., 1985, ApJ, 290, L35
- Grevesse N., 1989, in waddington C. J., ed, AIP Conf. Proc. Vol. 183, Cosmic Abundances of Matter, The Abundances of Matter in the Sun. Am. Inst. Phys., New York, p. 9
- Henning T., Mutschke H., 1997, A&A, 327, 743
- Henning T., Mutschke H., 2001, Spectrochim. Acta, 57, 815
- Hony S., Waters L. B. F. M., Tielens A. G. G. M., 2001, A&A, 378, L41
- Hony S., Waters L. B. F. M., Tielens A. G. G. M., 2002, A&A, 390, 533
- Hony S., Tielens A. G. G. M., Waters L. B. F. M., de Koter A., 2003, A&A, 402, 211
- Hrivnak B. J., Volk K., Kwok S., 2000, ApJ, 535, 275
- Hrivnak B. J., Volk K., Kwok S., 2009, ApJ, 694, 1147
- Huffman D., 1989, in Allamandola L. J., Tielens A. G. G. M., eds, IAU Symposium Vol. 135, Interstellar Dust. Kluwer, Dordrecht, p. 329
- Jiang B. W., Zhang K., Li A., 2005, ApJ, 630, L77
- Jiang B. W., Zhang K., Li A., 2009, Earth, Planets, and Space. in press (astro-ph/0812.2015)
- Jones A. P., Duley W. W., Williams D. A., 1990, Q. J. R. Astron. Soc., 31, 567
- Justanont K., Barlow M. J., Skinner C. J., Roche P. F., Aitken D. K., Smith C. H., 1996, A&A, 309, 612
- Kimura Y., Ishikawa M., Kurumada M., Tanigaki T., Suzuki H., Kaito C., 2005, J. Cryst. Growth, 275, 977
- Kimura Y., Kaito C., 2003a, J. Cryst. Growth, 255, 282
- Kimura Y., Kaito C., 2003b, MNRAS, 343, 385
- Kimura Y., Nuth J. A. III, Ferguson F. T., 2005, ApJ, 632, L159
- Kraus G. F., Nuth III J. A., Nelson R. N., 1997, A&A, 328, 419
- Koike C., Hasegawa H., Asada N., Hattori T., 1981, ApSS, 79, 77

- Kwok S., Volk K. M., Hrivnak B. J., 1989, *ApJ*, 345, L51
Kwok S., Volk K., Bidelman W. P., 1997, *ApJS*, 112, 557
Kwok S., Volk K., Hrivnak B. J., 1999, in Le Bertre T., Lebre A., Waelkens C., eds, *IAU Symp. 191, Asymptotic Giant Branch Stars*. Astron. Soc. Pac., San Francisco, p. 297
Kwok S., Volk K., Bernath P., 2001, *ApJ*, 554, L87
Kwok S., Volk K., Hrivnak B. J., 2002, *ApJ*, 573, 720
Lattimer J. M., Schramm D. N., Grossman L., 1978, *ApJ*, 219, 230
Li A., 2003, *ApJL*, 599, L45
Li A., 2008, in Mann I., Nakamura A., Mukai T., eds, *Lecture Notes in Phys. Vol. 758, Small Bodies in Planetary Sciences*. Springer-Verlag, Berlin, p. 167
Li M. P., Shi Q. J., Li A., 2008, *MNRAS*, 391, L49
Nuth J. A., Moseley S. H., Silverberg R. F., Goebel J. H., Moore W. J., 1985, *ApJ*, 290, L41
Oudmaijer R. D., de Winter D., 1995, *A&A*, 295, L43
Pierson H. O., 1996, *Handbook of Refractory Carbides and Nitrides: Properties, Characteristics, Processing and Applications*. Noyes Publications, Westwood, NJ
Posch T., Mutschke H., Andersen A., 2004, *ApJ*, 616, 1167
Radwanski R. J., Ropka Z., 2008, *Phys. B Condens. Matter*, 403, 1453
Reddy B. E., Lambert D. L., Gonzalez G., Yong D., 2002, *ApJ*, 564, 482
Roberts W. M., 1961, *Trans. Faraday Soc.*, 57, 99
Rouleau F., Martin P. G., 1991, *J. R. Astron. Soc. Can.*, 85, 201
Sourisseau C., Coddens G., Papoular R., 1992, *A&A*, 254, L1
Speck A. K., Hofmeister A. M., 2004, *ApJ*, 600, 986
Van Winckel H., Reyniers M., 2000, *A&A*, 354, 135
Volk K., Kwok S., Hrivnak B. J., 1999, *ApJ*, 516, L99
Volk K., Xiong G.-Z., Kwok S., 2000, *ApJ*, 530, 408
Von Helden G., Tielens A. G. G. M., van Heijnsbergen D., Duncan M. A., Hony S., Waters L. B. F. M., Meijer G., 2000, *Sci*, 288, 313
Voshchinnikov N. V., Henning T., 2008, *A&A*, 483, L9
Zhang K., Jiang B. W., Li A. G., 2006, *Prog. Astron. (Chin.)*, 24, 43
Zhukovska S., Gail H.-P., 2008, *A&A*, 486, 229

This paper has been typeset from a $\text{\TeX}/\text{\LaTeX}$ file prepared by the author.